Electrochemical Micromachining of p-Type Silicon†

P. Allongue,*,‡ P. Jiang, V. Kirchner, A. L. Trimmer,§ and R. Schuster

Fritz-Haber Institut der Max Planck Gesellschaft, Faradayweg 4-6, D-14195 Berlin, Germany

Received: January 19, 2004; In Final Form: May 24, 2004

Electrochemical micromachining (ECM) of p-type Si substrates is accomplished in HF-based solutions by applying nanosecond potential pulses between the substrate and a tungsten tool electrode. With sufficiently high potential pulses, the silicon potential locally reaches the electropolishing regime and microstructures may be machined. ECM precision is investigated as a function of pulse height, pulse duration, solution composition, and silicon doping level. Results show that micrometer precision may be obtained with highly doped substrates and that experimental data can be explained within a simple model, taking the charging time of the interface capacitance into account. In highly doped p-Si, well-defined microstructures can be realized without application of a mask on the surface. In addition, the isotropy of the process allows fabrication of structures not constrained by the crystal direction. In the case of low-doped material, ECM is only possible for very short pulses (<3 ns).

1. Introduction

The fabrication of MEMS (microelectromechanical systems) aims at developing "smart" products such as systems-on-a-chip, where mechanical components are combined with electronic circuitry in a miniaturized system. MEMS technology mostly relies on silicon micromachining, a well-established technology that combines lithography and etching steps, including wet anisotropic chemical etching or reactive ion etching.[1−4] In the case of wet etching, the highly orientation dependent dissolution reaction allows very smooth {111} planes to be revealed, since they are etch-stop planes in alkaline solutions.[5,6] Designers must hence imagine suitable masks and align them precisely with respect to the crystal axis to achieve their goal. One of the main difficulties, however, concerns the etching at convex and concave corners[1−4] where the intersection of two or more {111} planes generates complex and poorly controllable phenomena. So-called corner compensation remains a challenging question despite years of experience,[7−11] and the technique has proven to be an art more than a science. Therefore, the design of MEMS devices requires dedicated research efforts, including numerical simulations to predict etched shapes[4,10] and define suitable process sequences of fabrication.

Electrochemical dissolution of silicon was recently proven to be a useful technique for the machining of simple 3D microstructures in silicon substrates. The process is usually isotropic, and its speed is totally controlled by the current flow and may be adjusted with the applied potential (in the case of p-type substrate) or illumination level (in the case of n-type Si). High aspect ratio microstructures (macropores) were fabricated using prestructured very low doped n-type (100) substrates illuminated from the backside.[12−14] This approach relies on the preferential diffusion of photoholes toward pyramid tips (created by standard microfabrication techniques).[12] Pores propagate along the (100) direction, and a highly uniform pore diameter obtained for the process becomes self-limiting when the wall thickness reaches twice the thickness of the space-charge layer. High-performance 2D photonic band gap materials can be fabricated using this method.[13] Back illumination was recently replaced by using n-type Si electrodes with p−n junctions at the backside to inject holes instead of photoholes.[15]

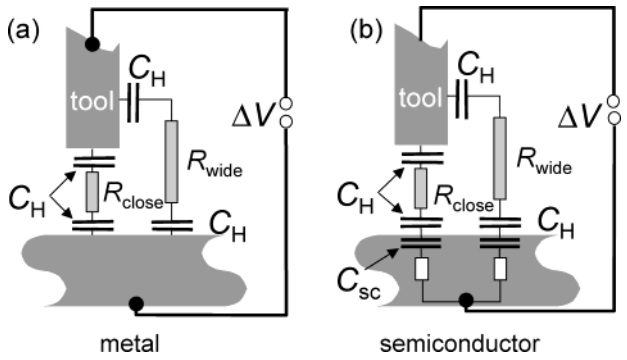

Figure 1. (a) Principle of the localization of electrochemical reactions by the application of short potential pulses in the case of a metal substrate. (b) Principle of the localization of electrochemical reactions by the application of short potential pulses in the case of a semiconductor substrate. See text for symbols.

In this contribution, we present an alternative electrochemical method, called electrochemical micromachining (ECM), using ultrashort voltage pulses, to machine silicon substrates in 3D without the application of a mask. The technique is based on the application of short potential pulses between a substrate and a tool electrode.[16] The reason for using *very short* pulses is obvious in the case of metal substrates as shown in Figure 1a. When a potential pulse (pulse amplitude ΔV, pulse width τ) is applied between the tool electrode and the substrate, the charging of the double-layer (DL) capacitance C_H occurs at both electrodes. When the substrate resistance is negligible in comparison with the solution resistance, the charging time constant τ_H of the DL capacitance is given by the product of C_H and the solution resistance R. ECM uses the fact that R and

† Part of the special issue "Gerhard Ertl Festschrift".

* To whom correspondence may be addressed. E-mail: pa@pmc.polytechnique.fr.

‡ Permanent address: Laboratoire de Physique de la Matière Condensée, CNRS UMR 7643, Ecole Polytechnique, F-91128 Palaiseau, France.

§ Permanent address: Department of Chemical Engineering, 102 Engineers' Way, PO Box 400741, University of Virginia, Charlottesville, Virginia, 22904.

10.1021/jp0497312 CCC: $27.50
Published on Web 07/03/2004

therefore also τ_H is distance dependent. $\tau_H(d) \approx \rho d C_H$, where d is the length of the current path in solution, i.e., the locally varying distance between the two electrodes. ρ is the solution resistivity. Reversing this argument, for a given pulse duration τ, the DL capacitance charging remains confined within distances where $\tau_H(d) < \tau$ or $d < P = \tau/\rho C_H$. Therefore, P estimates the distance between the electrodes, up to which significant electrochemical reaction can occur. In other words, in the case of electrochemical dissolution, P estimates the width of the gap between tool and work piece during ECM and is a measure for the machining precision. Its value depends only on pulse characteristics and solution resistivity. In 0.1 M H_2SO_4 solution, ($\rho \approx 50$ Ω.cm),[17] $P \approx 200$ nm for 10 ns long pulses (assuming $C_H = 10$ μF/cm^2). A metal workpiece can thus be machined in 3D by ECM with sub-micrometer precision and without applying a mask or covering the tool electrode with an insulating layer.[16] ECM of Cu, Co, Ni, Au, and steel has been recently demonstrated.[16,18−21] In the case of semiconductors (Figure 1b), the presence of an additional space-charge layer capacitance C_{SC} at the semiconductor/electrolyte interface as well as the non-negligible substrate resistance complicates the analysis. However, the underlying principle of ECM remains the same.

The present work demonstrates that p-type silicon ECM may be accomplished with good precision. The influence of pulse height, pulse duration, and solution composition are investigated in the case of highly doped silicon ECM. Results show that a precision better than 1 μm is obtainable. Examples of microstructures generated by ECM in highly doped p$^+$-Si(100) demonstrate that the method is reproducible and that the isotropy of the process overcomes problems related to micromachining at corners and mask alignment. However, the case of low-doped substrates is still a matter of concern due to the high substrate resistance and large extent of the space-charge layer. Therefore, machining of low-doped substrates with acceptable spatial resolution is only possible for pulse durations shorter than 3 ns.

2. Experimental Section

Electrochemical Micromachining. The experimental setup is described in detail in refs 16 and 18. The tool and workpiece potentials (U_{tool} and U_{Si}) are adjusted by use of a custom-made bipotentiostat. The corresponding counter and reference electrodes (not shown in Figure 1) were a Pt wire and a hydrogen-loaded Pd wire as quasireference. The high-frequency pulses were generated with a pulse generator (Hewlett-Packard 8314) and supplied to the tool via a home-built amplifier to account for the cell impedance. In the described experiments, pulse trains with a pulse-to-pause ratio of 1 to 10 were employed. Mechanical movement of the tool electrode was accomplished by a piezo-driven micromanipulator with strain gauges to monitor the absolute position. The zero distance between tip and surface was measured via controlled electric contact before the pulses were applied. During the experiment electric contact between the tool and the workpiece was avoided by sufficiently slow feed of the tool. For further experimental details, see ref 16.

Substrates, Tools, and Solutions. Silicon samples were cut from p-type Si(100) wafers of various resistivity purchased from Siltronix (France). Samples were cleaned in a hot mixture (H_2SO_4:H_2O_2) (2:1 by volume) and then copiously rinsed in ultrapure water. The oxide layer was then removed in 5% HF. After a final rinse in ultrapure water, a rear ohmic contact was realized by applying an In−Ga eutectic. Solutions were prepared using ultrapure water and electronic-grade chemicals. Three different solutions were used, the compositions of which are given in Table 1. Tool electrodes were made of tungsten. Starting from a 150 μm thick W wire, the first step consisted in preparing a sharp tip by electrochemical etching in 2 M NaOH similar to the preparation of STM tips. When required, flat-bottomed, nearly cylindrical tools were obtained from the sharp STM tips by insulation of the tip shaft with Apiezon wax and subsequent removal the uncovered part of the tip by electrochemical etching in 2 M NaOH.

TABLE 1: Composition and Resistivity of the Solutions Used for ECM of Si and Slope S of the Experimentally Determined Gap Width−Pulse Width Curves, Measured for 1.5 V-Pulses in p$^+$ Si

solution	composition	ρ (Ω·cm)[17]	S/μm ns^{-1}
A	5 M HF + 0.1 M H_2SO_4	7	0.83/1.06[a]
B	1 M HF	31.7	0.27
C	1 M HF + 1 M NH_4F	<32	0.65

[a] Measured after KOH etch to remove porous silicon.

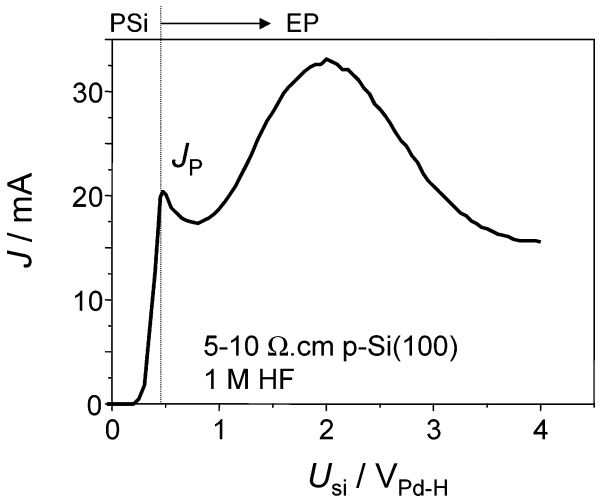

Figure 2. Typical current−voltage curve of a p-Si(100) electrode in 1 M HF. At polarizations lower than $U_{peak} = 0.5$ V, porous Si (PSi) is formed on the electrode. For $U_{Si} > U_{peak}$, the Si electrode dissolves in the electropolishing regime (EP). Therefore, ECM in this solution requires pulses such that the electrode potential exceeds 0.5 V near the tool electrode. U_{Si} is referenced vs a Pd/H electrode.

3. Results and Discussion

3.1. Electrochemical Conditions. Upon polarization, the p-Si/solution interface behaves similar to a diode with the solution playing the role of the metal contact. This behavior is illustrated by the cyclic voltammogram of p-type Si(100) in 1 M HF solution shown in Figure 2, the typical shape of which resembles previously published curves.[22] Upon scanning U_{Si} toward potentials larger than the open circuit potential (OCP), the potential barrier decreases inside silicon and holes (h$^+$) thermally jump over it and are captured in surface bonds leading to silicon dissolution according to the simplified overall reactions[23]

$$Si + 2h^+ \rightarrow Si^{2+} \quad (1a)$$

$$Si^{2+} + 2H^+ \rightarrow Si^{4+} + H_2 \quad (1b)$$

or

$$Si + 4h^+ \rightarrow Si^{4+} \quad (2)$$

The above reactions are *symbolic* reactions that skip the details of complex mechanisms on the molecular scale. For more

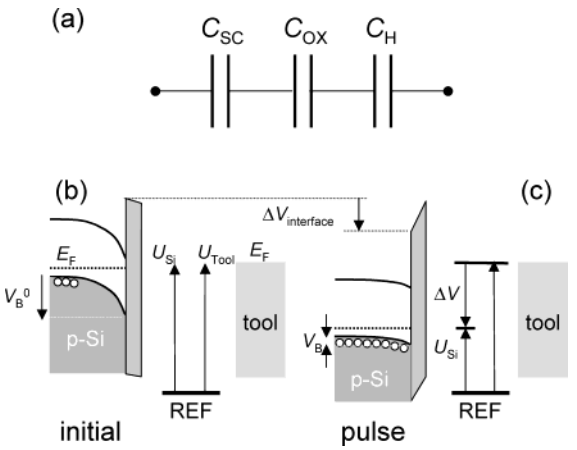

Figure 3. (a) Equivalent capacitance of the Si−solution under anodic polarization inside the electropolishing regime. C_{SC} is the space-charge layer capacitance, C_{OX} corresponds to the oxide layer, and C_H corresponds to the DL. (b) Energy diagram of the Si−solution interface in the vicinity of the tool without applied voltage. V_B denotes the band bending. (c) Same as part b upon application of a pulse of amplitude $\Delta V > 1$ V. Note that the applied voltage ΔV leads to a change of the band bending ΔV_B and a potential drop across the interface $\Delta V_{interface}$.

details, the reader may refer to models published by different authors.[23−25] Reaction 1 occurs for $0 < U_{Si} < U_{peak} = 0.5$ V, i.e., on the left-hand side of the sharp peak marked with the dotted line. It is a divalent two-step reaction in which the second oxidation step occurs in solution and leads to molecular hydrogen (bubbles are visible to the naked eye on the electrode surface when $U_{Si} < 0.5$ V). In this dissolution regime, also called porous silicon formation regime (PSi), the heterogeneous dissolution leads to the formation of a sort of silicon sponge while the optical surface plane remains at its initial level. For $U_{Si} > 0.5$ V, reaction 2 takes place. It is tetravalent since the silicon surface becomes covered by a thin oxide layer (no hydrogen is formed). In this dissolution regime, also called the electropolishing (EP) regime, the dissolution is homogeneous and leads to a smooth surface state. The intensity J_P of the peak current, which marks the transition between porous silicon formation and electropolishing, depends essentially on solution composition (HF concentration and pH)[26] and little on substrate orientation. Increasing the doping level smears out the first peak. From Figure 2, we conclude that ECM will require that U_{Si} has to locally exceed $U_{peak} = 0.5$ V upon application of potential pulses, otherwise PSi will be formed.

The equivalent capacitance C_{EQ} of the Si−solution interface under anodic polarization is the series combination of the three capacitances shown in Figure 3a, i.e., the space-charge capacitance of the semiconductor surface C_{SC}, the capacitance of an oxide layer C_{OX}, formed during the dissolution of the silicon in the electropolishing regime, and the usual Helmholtz capacitance C_H at the surface−electrolyte interface. The space-charge capacitance of depleted p-Si is given by $C_{SC} = (q\epsilon_{Si}\epsilon_0 N_A/2)^{1/2}\cdot(V_B)^{-1/2}$,[27] with N_A the volume concentration of acceptor atoms and V_B the band bending inside silicon and all other symbols having their usual meaning ($\epsilon_{Si} = 11.9$).[27] To give an order of magnitude, $C_{SC} = 18$ nF/cm^2 for 5−10 Ω·cm p-type silicon and 1.8 μF/cm^2 for 5 mΩ·cm p-type silicon (both capacitances calculated for $V_B = 0.5$ V). Under a steady state, planar electropolishing conditions Fonseca et al.[28] found that the oxide thickness is varying linearly with the applied overpotential. For an applied polarization of 1−2 V, a thickness of 1−2 nm has to be expected. However, in our experiments, the potential is pulsed with a pulse-to-pause ratio of 1/10, which should

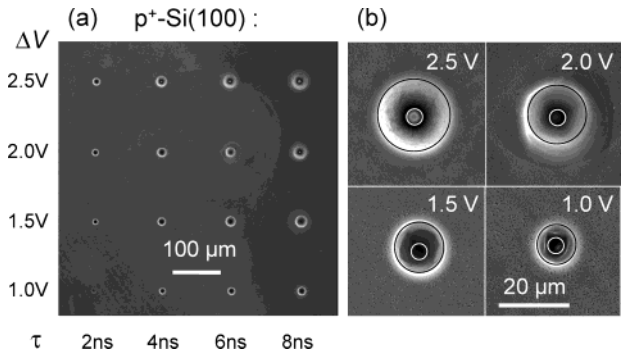

Figure 4. (a) SEM images of holes drilled in 5 mΩ·cm p-Si(100) in contact with 5 M HF + 0.1 M H_2SO_4. The pulse amplitude and duration are indicated in the figure. (b) SEM images of individual holes obtained with 4-ns pulses at various voltages as indicated. Black and white circles correspond to the diameter of the edge of the hole $Ø_{hole}$ and that of the tip $Ø_{tip}$ ($Ø_{tip} = 4.4$ μm in this experiment).

diminish the thickness of the oxide layer in comparison with steady-state electropolishing conditions. For a 1 nm thick SiO_2 layer ($\epsilon_{SiO_2} = 3.9$),[23] the capacitance $C_{OX} = \epsilon_{SiO_2}\epsilon_0/d_{OX} = 3.45$ μF/cm^2 is calculated. The value of the DL capacitance C_H on *oxidized* silicon has not been measured, to our knowledge. We assume it to be $C_H = 10$ μF/cm^2.

The initial energy diagram of the p-Si−electrolyte junction is depicted in Figure 3b for $U_{si} \approx 0$ V and $U_{tool} \approx 0$ V vs Pd/H reference (see experimental). The band bending amounts to about $V_B^0 \approx 1$ V,[29] and the Si surface is under strong depletion. Upon application of a voltage pulse between the Si and the tool electrode, the pulse voltage will mainly drop across the silicon−solution interface, since the DL capacitance at the tool electrode (assumed equal to 10 μF/cm^2) is much greater than the equivalent capacitance of the silicon electrode (series combination of C_{Si} and C_{OX}) even for highly doped silicon. Therefore, upon application of a moderate voltage pulse with amplitude $\Delta V < 1$ V, the Si remains under depletion the applied pulse voltage ΔV mainly leads to a decrease of the band bending by ΔV_B, i.e., $\Delta V = -\Delta V_B$ ($\Delta V_B < 0$). For $\Delta V > 1$ V, strong hole accumulation might be expected, but the corresponding high density of surface charge induces a reorganization of the potential distribution across the Si−solution interface with a shift of the band edges with respect to the reference in solution. The energy diagram during application of such a potential pulse is shown in Figure 3c, where $\Delta V = -\Delta V_B + \Delta V_{interface}$, with $\Delta V_{interface}$, the potential drop across the "interface" region comprising the DL region *and* the eventual oxide layer at the silicon surface. As explained above, note that the Fermi level of the tool electrode remains nearly unchanged during application of the pulse because the DL capacitance is greater on the tool than the equivalent capacitance of the silicon electrode.

3.2. ECM of Highly Doped Substrates (5 mΩ·cm) p-Si-(100). Figure 4a presents a scanning electron microscopy (SEM) image of an array of 10 μm deep holes drilled in 5 M HF + 0.1 M H_2SO_4 (solution A) using pulses of various length and amplitude, as indicated in the figure. Processing time was ca. 4 min per hole. The 4 × 4 matrix shows that the hole diameter (measured on the surface plane) is increasing with pulse amplitude ΔV for fixed pulse width τ. Similarly the hole diameter increases with τ for a given ΔV. As can be inferred from close-up images in Figure 4b, the shape of holes drilled with 4-ns pulses reproduces fairly well the tip shape (truncated cone of diameter 4.5 μm at 10 μm from the tip extremity). The inner walls of the holes are quite smooth for 1.5 V $< \Delta V <$ 2 V while they are rough for $\Delta V = 2.5$ and 1 V. This effect

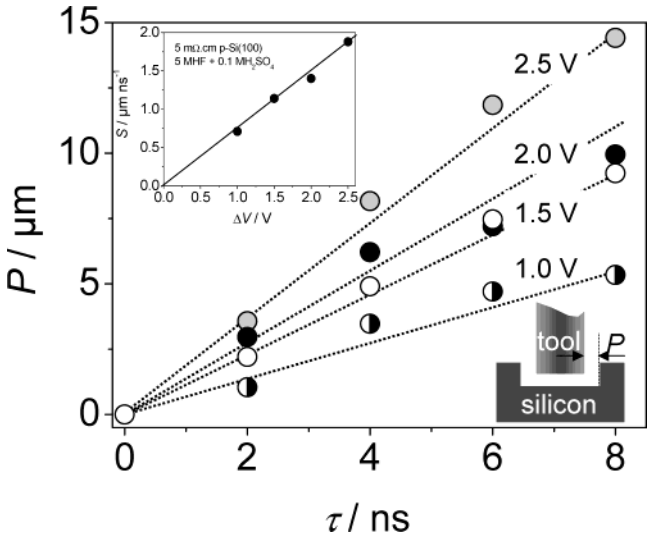

Figure 5. Plots of the gap width P between the edge of the hole and the tool electrode (see scheme) as a function of τ for various values of ΔV as indicated in the figure. Note the linear variations (slope S). Data are taken from Figure 4. Inset: plot of the slope S as a function of ΔV.

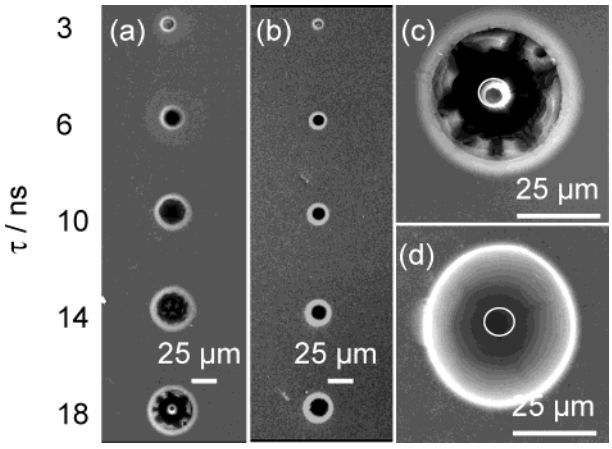

Figure 6. (a) SEM images of holes drilled in 5 mΩ·cm p-Si(100) in 5 M HF + 0.1 M H_2SO_4. Each hole is 20 μm deep and was machined within 9 min ($\Delta V = 1.5$ V, the pulse width τ is indicated in the figures). (b) SEM images of holes drilled in 5 mΩ·cm p-Si(100) in 1 M HF + 0.1 M H_2SO_4. Holes are 10 μm deep and were drilled in 18 min. (c,d) SEM images of the hole formed with 18-ns pulses in 5 M HF + 0.1 M H_2SO_4 (see a) before and after KOH etch.

becomes more and more obvious as the pulse width increases. In Figure 5, the gap width P between the tool and the substrate (see Scheme) is plotted vs the pulse duration. In practice, P is measured as $[\text{Ø}_{\text{hole}} - \text{Ø}_{\text{tip}}]/2$, with Ø_{hole} the hole diameter measured on the surface plane and $\text{Ø}_{\text{tip}} = 4.5$ μm. P characterizes the precision of ECM. For a given pulse height, as indicated in the figure, we find that the gap width P varies linearly with the pulse width τ, with a slope S (the dotted straight lines are linear regression plots forced to pass through the origin). The plot given in inset shows that the slope S varies almost linearly with ΔV.

In Figure 6 we compare two series of holes drilled in 5 M HF + 0.1 M H_2SO_4 (solution A) and 1 M HF (solution B) using 1.5-V pulses of increasing duration. The tip was nearly a cylinder of diameter 9.1 μm. ECM time was 9 min per 20 μm deep hole in solution A (Figure 6a) and 18 min per 10 μm deep hole in solution B (Figure 6b). The value of τ is indicated on the left of the figure. Holes drilled in solution B showed always smoother inner walls and sharper edges than those formed in solution A. The roughening of walls in solution A is particularly

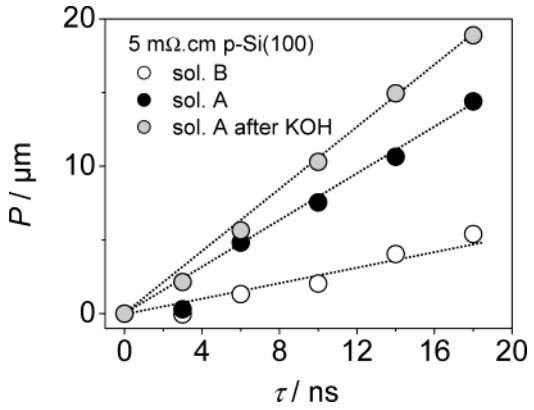

Figure 7. Plots of the gap width P as a function of the pulse width τ in 1 M HF (solution B, open symbols) and 5 M HF + 0.1 M H_2SO_4 (solution A, filled symbols) for a 5 mΩ·cm p-Si(100) workpiece. Solution A with lower resistivity yields higher P values. In the case of solution A, the gap width P before (black circles) and after removal of porous silicon by KOH etch (gray circles) is depicted.

visible as τ increases (Figure 6c). However, after 2 min etching in 2 M KOH, the same hole slightly widens and its walls appear very smooth (Figure 6d), suggesting that porous silicon was covering walls after initial ECM. Plots of the gap width P between the tool and hole edge vs the pulse width τ (Figure 7) derived from this experiment evidence again linear variations of P with the pulse width. The slope S increases from 1 M HF (solution B) to 5 M HF + 0.1 M H_2SO_4 (solution A). In other words, at the same pulse width, machining in the solution with the higher resistivity yields the smaller gap width P.

Since the substrate resistivity of highly doped Si is smaller than that of the electrolyte, the basic expression for the precision, $P \approx \tau/(\rho C_H)$, used with metal substrates can reasonably be applied to the highly doped semiconductor case by replacing C_H by the equivalent capacitance C_{EQ} (Figure 3a). Within this simple model, P is estimated by

$$P \approx \tau/(\rho C_{EQ}) = S\tau \qquad (3)$$

The linearity of the $P-\tau$ plots (Figures 5 and 7) and the higher values of the constant of proportionality S for the lower resistivity of the electrolyte (solution A) are in qualitative agreement with eq 3. Also quantitatively the experimental S values given in Table 1 are easily accounted for, assuming $C_{EQ} \approx C_{SC}$: Neglecting that the band bending changes during the application of the pulse upon polarization of the Si−electrolyte interface and employing an intermediate value of $V_B = 0.5$ V yields $S \approx 0.25$ μm/ns with $\rho = 30$ Ω·cm (solution B) and 1.10 μm/ns for $\rho = 7$ Ω·cm (solution A). These values are in excellent agreement with the experimental ones, determined for pulse amplitudes of 1.5 V, though we have neglected the presence of the oxide layer, which might slightly change the value of the equivalent capacitance C_{EQ}. Figure 5 shows that the gap width P increases with increasing ΔV and the plot in inset demonstrates that the slope S of the $P-\tau$ curves varies linearly with ΔV (Figure 8). This suggests that the ECM precision is indeed affected by the presence of a surface oxide layer: As discussed above, the band bending is essentially independent of applied voltage under electropolishing conditions (Figure 3c). At completely polarized regions of the workpiece, i.e., in close proximity of the tool electrode where the polarization really reaches approximately the applied pulse voltage, increasing pulse amplitude ΔV promotes linear variations of the oxide thickness t_{OX} in analogy with steady-state electropolishing.[28] This simple model seems consistent with the experimental

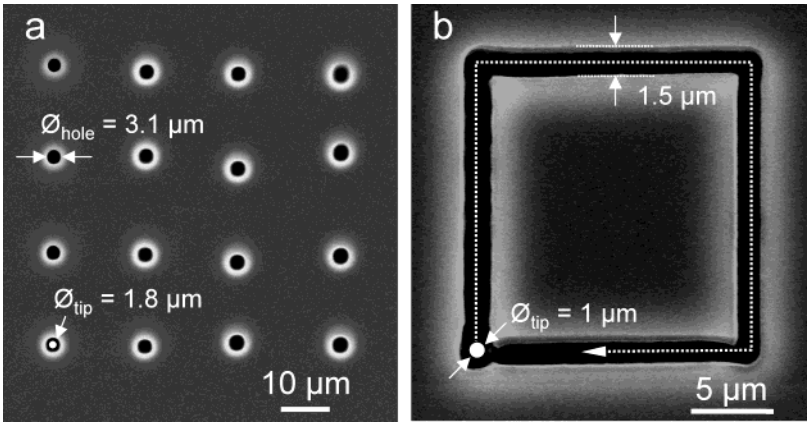

Figure 8. (a) SEM image of a 4 × 4 array of 15 μm deep holes drilled in 1 M HF + 1 M NH_4F. Note the reproducibility of processing. Pulses are 6 ns long and 1.5 V high. The tip diameter was 1.8 μm, the machining time arose to 1 min per hole. (b) SEM view of a square microstructure generated in solution B (τ = 6 ns, ΔV = 1.5 V). First a 5 μm deep hole was drilled with a W tip (diameter 1 μm) before moving it laterally along the indicated path (see dotted line). Note the sharp edges and well-defined shape of the trough, even at the corners (total machining time = 65 min).

increase of S with increasing pulse amplitude ΔV (Figure 5, inset). Reality is, however, more complex than this simple model because the gap width P is determined by the distance from the tool, where the reaction rate drops to (about) zero, i.e., where the local polarization is too low to dissolve the silicon at a significant rate (the transition corresponds probably to regions where the polarization is ~0.5 V (see Figure 2). Therefore, upon application of higher voltage pulses, this "threshold voltage" is shifted to further distances from the tool electrode, which is in agreement with the observation. However, a quantitative explanation of Figure 5 would require detailed knowledge on the potential dependent local polarization and the corresponding reaction rates.

From the data above, a micrometer precision is obtained with 6-ns potential pulses of ΔV = 1.5 V in 1 M HF. By use of such potential pulses, in Figure 8 we present two examples of microstructures machined in p^+-Si(100) without applying a mask. The 4 × 4 hole array (Figure 8a) was obtained in 1 M HF + 1 M NH_4F. Each 15 μm deep hole was drilled in 1 min. Their mean diameter of 3.1 μm corresponds to a gap width P = 0.65 μm between the tip and the edge of the hole (tip diameter ≈ 1.8 μm). One notes that ECM is easily reproducible, which implies that the W tool is not significantly altered during processing. Figure 8b presents an SEM view of a square microstructure generated in 1 M HF by first drilling a hole (5 μm deep) with the W tool (Ø$_{tip}$ = 1 μm, see white disk) and then moving the tool laterally along the indicated path to remove material similar to a milling machine. The total ECM time was 65 min because lateral motion of the tool was kept slow enough to avoid electrical contact with the substrate. This structure shows again how controllable ECM is. The trough width is fairly uniform and equals about 1.5 μm on average. Its edges are also considerably sharp. Furthermore, it is remarkable that this result is obtained without paying attention to the crystal orientation. In addition, ECM can easily obtain convex, right-angled corners. This demonstrates one advantage of ECM over conventional micromachining, since such a kind of microstructures with convex corners are not easily obtainable with techniques such as wet chemical etching.[1−11] Additionally, wet chemical etching is impossible with highly doped Si due to etch stop processes.

3.3. ECM of Low-Doped Substrates (5−10 Ω·cm) p-Si(100). In 5 M HF + 0.1 M H_2SO_4 solution, "pushing" the tool inside low-doped p-Si(100) proved to be almost impossible, suggesting that no significant dissolution occurred. In contrast, in 1 M HF, drilling was possible, and Figure 9 shows two attempts for drilling holes with 3- and 14-ns pulses with ΔV =

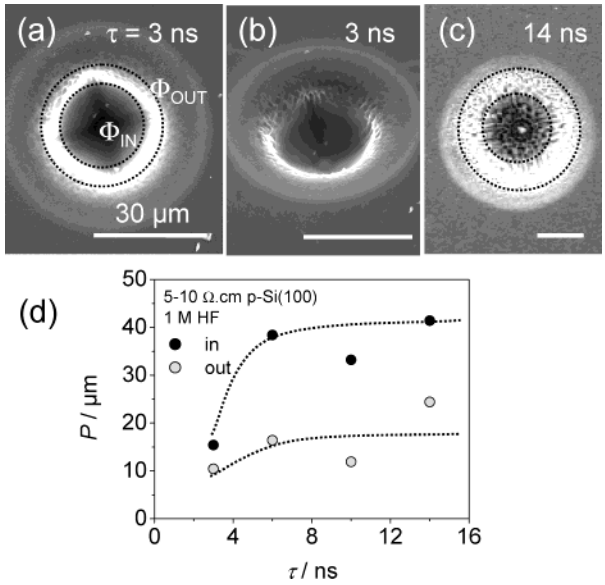

Figure 9. Planar (a) and tilted (b) SEM views of a 1 μm deep hole drilled in 5−10 Ω·cm p-Si(100) in 1 M HF (τ = 3 ns, ΔV = 1.5 V). (c) same as (a) for τ = 14 ns. The scale bar is 30 μm in all images. (d) Plot of the gap width P_{out} and P_{in} for the outer and inner edges of the hole as a function of τ. Data at τ = 3 and 14 ns correspond to parts a and c.

1.5 V. A rather well defined 1 μm deep hole could be realized with 3-ns pulses (see top and tilted SEM views, parts a and b of Figure 9). The inner walls are pretty smooth even though the SEM images evidence also a porous region of diameter 32 μm (measured on the surface plane), whereas the diameter of the smooth hole is only 22 μm (as measured a few μm below the surface plane). Note that both values are much larger than the tip diameter (Ø$_{tip}$ = 1.2 μm as measured 1 μm from the tip extremity). With 14-ns pulses, only porous silicon formation is observed over much larger distances (Figure 9c). Two characteristic diameters Ø$_{out}$ and Ø$_{in}$ corresponding to two different porous morphologies may be defined. Inside Ø$_{in}$, the surface is slightly depressed and smoother than outside where highly porous silicon is observed without formation of a depressed region. Figure 9d plots P_{out} = [Ø$_{out}$ − Ø$_{tip}$]/2 and P_{in} = [Ø$_{in}$ − Ø$_{tip}$]/2 as a function of τ. Converse to the p^+ silicon case, P does not vary linearly with the pulse width (dotted lines are just guide to eye) and takes much larger values than in Figures

5 and 7. Even when $\tau = 3$ ns, the ECM precision is $P_{in} \approx 10$ μm, which is 10 times larger than the value for highly doped silicon.

By use of eq 3 and taking into account the fact that $C_{EQ} \approx C_{SC} \approx 30$ nF/cm^2 for $V_B = 0.2$ V, a gap width of $P \approx 33$ μm is expected for 3-ns pulses. This value is larger than the 10 μm measured experimentally (Figure 9d). Equation 3 is also unable to predict that P saturates for $\tau > 6$ ns (Figure 9d) and that mainly porous silicon is formed at pulse durations exceeding 6 ns. These observations indicate that the polarization of the low-doped p-Si−solution interface remains too low to achieve dissolution in the electropolishing regime. The reason has to be sought in the relatively high specific substrate resistance, which is comparable to that of the solution. Hence, part of the potential drop is expected to occur in the substrate, and the simple model above, which assumes an infinitely low substrate resistance, is not valid anymore. However, in the limiting case of very short pulses, when the radius of the charged areas becomes small, charging of the DL should become possible even for high-resistance substrates, due to the hemispherical current flow in the substrate: Analogous to the charging behavior of the DL at an Ultra Micro Electrode, the time constant for the DL charging is decreasing linearly with the diameter of the charged area. Vice versa, with short enough pulses and therefore small enough charged areas, the polarization of the substrate should become high enough to allow for Si dissolution. In our experiment, hole drilling becomes possible for pulse durations below about 6 ns. A detailed model had to include the time-dependent, local charging of the substrate−solution interface with finite resistance of both, substrate and solution, and is beyond the scope of this paper. It should be noted at this point that with low-doped silicon further complications might come into play. For example, the space-charge layer thickness becomes about 1 μm, which gives the minimum length scale for potential variations on the surface. With 3-ns pulses this length is, however, still below the achieved machining precision of $P \approx 10$ μm.

5. Conclusion

We have demonstrated that electrochemical machining of p-Si substrates may be accomplished in an HF-based solution using nanosecond pulses applied between the substrate and a tungsten tool electrode. The process is maskless and does not require insulation of the tool electrode. A critical point of the method is the optimization of the electrolyte to allow sufficiently fast dissolution without degrading too much the precision of machining. In addition, the potential pulse must be sufficiently large to polarize the silicon surface into the electropolishing regime of the cyclic voltammogram and avoid porous silicon formation. We have obtained sub-micrometer precision with highly doped substrates, and experimental data could be rationalized within a simple model considering local DL capacitance charging. In the case of low-doped material, ECM is possible for very short pulses (<3 ns), and a machining precision of 10 μm was achieved. Although the method needs to be optimized, in particular to increase the machining speed, it should nevertheless find interesting applications, since the machining proceeds isotropically and allows for the fabrication of well-defined microstructures with sharp corners.

Acknowledgment. This work was partially supported by the German-French bilateral cooperation program Procope (Contract 04480VM) and the Center for Nanoscopic Materials Design, a National Science Foundation Materials Research Science and Engineering Center at the University of Virginia.

References and Notes

(1) Lang, W. *Mater. Sci. Eng.* **1996**, *R17*, 1.

(2) McWhorter, P. J.; Frazier, A. B.; Rai-Choudhury, P. In *Handbook of Microlithography, Micromachining and Microfabrication*; Rai-Choudhury, P., Ed.; Society of Photo-Optical Instrumentation Engineers: Bellingham, WA, 1997; Vol. 2, pp 3−40.

(3) Kovacs, G. T. A.; Maluf, N. I.; Petersen, K. E. *Proc. IEEE* **1998**, *86*, 1536.

(4) Elwenspoek, M. C.; Jansen, H. V. *Silicon Micromachining*; Cambridge University Press: Cambridge, 1998.

(5) Williams, K. R. *J. Microelectromech. Syst.* **1996**, *5*, 256.

(6) Seidel, H.; Csepregi, L.; Baumgärtel, A. *J. Electrochem. Soc.* **1990**, *137*, 3612.

(7) Shikida, M.; Nanbara, K.; Koizumi, T.; Sazaki, H.; Odagaki, L.; Sato, K.; Ando, M.; Furuta, S.; Asaumi, K. *Sens. Actuators, A* **2002**, *97*−*98*, 758.

(8) Horn, A.; Schröder, H.; Obermeier, E.; Wachutka, G. Proceedings of 3rd International Conference on Modeling and Simulation of Microsystems. *Sensors and Actuators (MSM 2000)*; San Diego, CA, 2000; pp 63−66.

(9) Oosterbroek, R. E.; Berenschot, J. W.; Jansen, H. V.; Nijdam, A. J.; Pandraud, G.; van den Berg, A.; Elwenspoek, M. C. *J. Microelectromech. Syst.* **2000**, *9*, 1057.

(10) Zhang, Q.; Liu, L.; Li, Z. *Sens. Actuators, A* **1996**, *56*, 251.

(11) Nikpour, B.; Landsberger, L. M.; Kahrizi, M.; Iftimie, A. *Sens. Actuators, A* **1998**, *66*, 299.

(12) Lehmann, V. *J. Electrochem. Soc.* **1993**, *140*, 2836.

(13) Grünig, U.; Lehmann, V.; Ottow, S.; Busch, K. *Appl. Phys. Lett.* **1996**, *68*, 747.

(14) Kleimann, P.; Linnros, J.; Juhasz, R. *Appl. Phys. Lett.* **2001**, *79*, 1717.

(15) Badel, X.; Linnros, J.; Kleimann, P. *Electrochem. Solid-State Lett.* **2003**, *6*, C79.

(16) Schuster, R.; Kirchner, V.; Allongue, P.; Ertl, G. *Science* **2000**, *289*, 98.

(17) Dobos, D. In *Electrochemical data*; Elsevier Science: Amsterdam, 1975.

(18) Kock, M.; Kirchner, V.; Schuster, R. *Electrochim. Acta* **2003**, *48*, 3213−3219.

(19) Cagnon, L.; Kirchner, V.; Kock, M.; Schuster, R.; Ertl, G.; Gmelin, W. T.; Kück, H. *Z. Phys. Chem.* **2003**, *217*, 299−313.

(20) Kirchner, V.; Cagnon, L.; Schuster, R.; Ertl, G. *Appl. Phys. Lett.* **2001**, *79*, 1721.

(21) Trimmer, A. L.; Hudson, J. L.; Kock, M.; Schuster, R. *Appl. Phys. Lett.* **2003**, *82*, 3327−3329.

(22) For a review on porous silicon formation and applications, see: Formation mechanisms of porous silicon. *EMIS Datareview Series, Properties of Porous Sicilon*; Canham, L., Ed.; Institution of Electrical Engineers: London, 1997; Chapter 1.1, Vol. 18, pp 3−12.

(23) Zhang, X. G. In *Electrochemistry of silicon and its oxide*; Kluwer Academic/Plenum Publishers: New York, 2001.

(24) Searson, P. C. In *Advances in Electrochemical Science and Engineering*; Gerischer, H., Tobias, C. W., Eds.; VCH: Weinheim, 1995; Vol. 4, Chapter 2, p 69.

(25) Allongue, P.; Costa-Kieling, V.; Gerischer, H. *Electrochim. Acta* **1995**.

(26) Hassan, H. H.; Sculfort, J. L.; Etman, M.; Ozanam, F.; Chazalviel, J.-N. *J. Electroanal. Chem.* **1998**, *380*, 55.

(27) Morrison, S. R. In *Electrochemistry at Semiconductor and Oxidized Metal Electrodes*; Plenum Press: New York, 1980.

(28) da Fonseca, C.; Ozanam, F.; Chazalviel, J.-N. *Surf. Sci.* **1996**, *365*, 1.

(29) Gorostiza, P.; Allongue, P.; Diaz, R.; Morante, J. R.; Sanz, F. *J. Phys. Chem. B* **2003**, *107*, 6454.